Biophysical Journal Volume 71 November 1996 2394–2403

Modeling the Attenuation and Failure of Action Potentials in the Dendrites of Hippocampal Neurons

M. Migliore
National Research Council, Institute for Interdisciplinary Applications of Physics, 90123 Palermo, Italy

ABSTRACT We modeled two different mechanisms, a shunting conductance and a slow sodium inactivation, to test whether they could modulate the active propagation of a train of action potentials in a dendritic tree. Computer simulations, using a compartmental model of a pyramidal neuron, suggest that each of these two mechanisms could account for the activity-dependent attenuation and failure of the action potentials in the dendrites during the train. Each mechanism is shown to be in good qualitative agreement with experimental findings on somatic or dendritic stimulation and on the effects of hyperpolarization. The conditions under which branch point failures can be observed, and a few experimentally testable predictions, are presented and discussed.

INTRODUCTION

The important function of a dendritic tree in conveying external inputs to the soma and somatic activity back to dendrites cannot be overemphasized. In general, it can be expected that, besides the static filtering action of a passive dendritic tree, the properties of the dendritic membrane can significantly distort the transmission of a synaptic input (Wilson, 1995) or modulate the propagation of an action potential throughout the cell (Andreasen and Lambert, 1995; Spruston et al., 1995; Callaway and Ross, 1995).

Recent experimental advances using simultaneous somatic and dendritic recordings from hippocampal CA1 neurons (Spruston et al., 1995) have shown that the active properties of dendrites can change the amplitude of the action potentials (APs) in the dendrites in an activity-dependent manner. In particular, when a train of APs was elicited by a somatic or dendritic current injection, a progressive reduction of the amplitude of the APs was observed during the train and along the major apical dendritic trunk. This effect was clearly evident at about 150 μm and was dramatic beyond 300 μm from the soma (see Fig. 2 of Spruston et al., 1995), where the ratio of the AP amplitude of the last to the first AP in the train was as low as 0.1. Often in distal dendrites a failure (i.e., an abrupt reduction) rather than a gradual attenuation of the AP amplitude was observed, and in several cases the failure was localized after a major branch point. The time to recover the full amplitude of a test AP in distal dendrites was shown to depend on prior conditioning. In fact, suprathreshold depolarization resulted in attenuation of the AP amplitude, whereas a subthreshold stimulation did not. Furthermore, the amplitude of a test AP remained small for a longer time (about 1 s) when more APs were elicited during conditioning, and hyperpolarization accelerated the recovery time.

Experiments, however, have not been paralleled by the development of a clear model of the mechanisms that could be involved with these effects. The voltage dependence and time constants that appear to be involved with the experimentally observed AP changes are not embodied in the standard HH-like models used to reproduce the main firing characteristics of CA1 hippocampal neurons (e.g., Traub and Llinás, 1979; Warman et al., 1994). In particular, the voltage dependence of the time constant involved with the changes in the AP amplitude (on the order of seconds near the resting potential and much faster for both hyperpolarized and depolarized potentials) is not found in the "classical" Na^+, Ca^{2+}, or K^+ channel kinetics. A model lacking this critical feature cannot reproduce the attenuation or failure as observed in the experiments. New mechanisms are thus needed. There are two major, and conceptually different, classes of mechanisms that could be responsible for these effects: an activity-dependent reduction in the sodium current, and a dynamical change in the shunting properties of the dendritic membrane. A slow inactivation of the sodium current has been originally described in the *Myxicola* giant axons (Rudy, 1981), whereas various time- and/or voltage-dependent conductances (such as those controlling inhibition) could dynamically change the shunting properties of the membrane (Wall, 1995). Our aim is to present two physiologically reasonable mechanisms, one for each class, and to show that they are independently consistent with experimental findings for CA1 pyramidal neurons, suggesting that one or both of these mechanisms could underlie the activity dependence of the back-propagation of action potentials in the dendritic tree.

Received for publication 6 February 1996 and in final form 29 July 1996.
Address reprint requests to Dr. M. Migliore, CNR-IAIF, via Archirafi 36, 90123 Palermo, Italy. Tel.: +0039-91-6233209; Fax: +0039-91-6162480; E-mail: michele@risc2.iaif.pa.cnr.it.

0006-3495/96/11/2394/10 $2.00

METHODS

We performed our simulations with the program NEURON (version 3.0) (Hines, 1993) on a DEC 3000/400 workstation, using a 20-μs time step. This time step resulted in no

significant differences in preliminary test simulations when time steps as low as 2 μs were used. Typical run times were 5 min of CPU time for 1 s of simulation. We used a simplified geometry of a CA1 hippocampal neuron, composed of 98 segments, grouped in 16 compartments: one for the axon, one for the soma, three for basal dendrites, and 11 for apical dendrites (Fig. 1 *A*). An intracellular resistivity of $R_a = 200$ Ωcm and a membrane time constant of $\tau_m = 28$ ms were used, as suggested by experiments (Spruston and Johnston, 1992). To account for spines and small dendritic branches that were not modeled explicitly, the more conventional values for $R_m = 28000$ Ωcm^2 and $C_m = 1$ μF/cm^2 were changed to $R_m = 8000$ Ωcm^2 and $C_m = 3.5$ μF/cm^2, to effectively increase the membrane area. With these values, an input resistance of $R_N \approx 100$ MΩ resulted for our model cell. Active conductances were distributed on axon, soma, basal, and most of the apical dendrites, as shown in Fig. 1 *A* (*darker lines*).

The general formalism used to model the voltage dependence of most of the gating variables derives from the HH-like scheme proposed by Borg-Graham (1991), where the expressions for α_x, β_x, x^∞, and τ_x are

$$\alpha_x = \alpha_0 \exp(-\gamma z(V - V_{1/2})F/RT)$$

$$\beta_x = \beta_0 \exp((1 - \gamma)z(V - V_{1/2})F/RT)$$

$$x_\infty = \alpha_x/(\alpha_x + \beta_x) \qquad \tau_x = 1/(\alpha_x + \beta_x),$$

where V is the membrane potential (in mV); $\alpha_0 = \beta_0 =$ constant; z, γ, and $V_{1/2}$ are the model parameters for the gating variable x; F is Faraday's constant; R is the gas constant; and T is the absolute temperature.

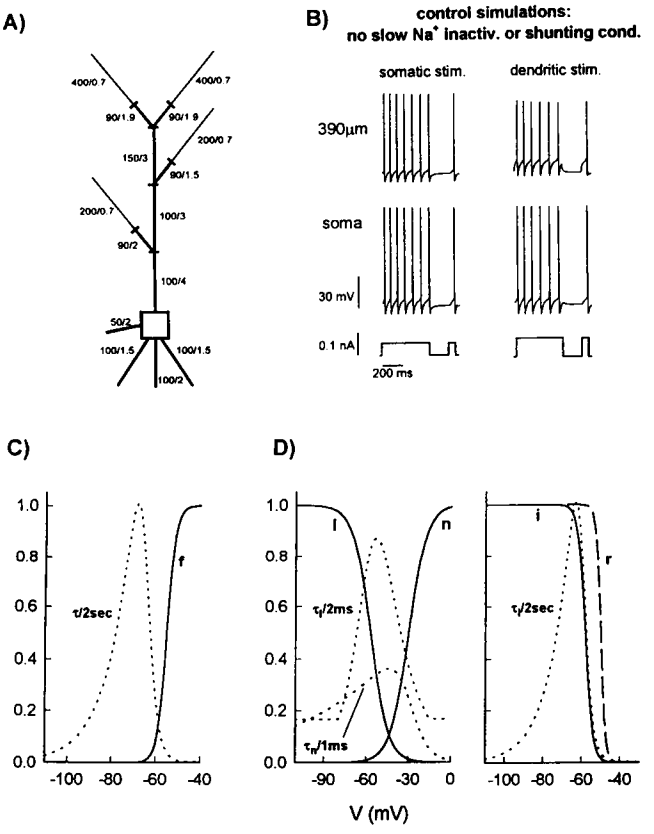

FIGURE 1 (*A*) The model cell we used in all simulations. For each compartment, the length and diameter are given in microns. Darker lines represent compartments where active conductance has been distributed. (*B*) Simulations of control conditions, without the slow sodium inactivation or the shunting conductance. Membrane potential is shown at the soma (*lower traces*) and at 390 μm (*upper traces*). A train of APs was generated with a 500-ms current injection of 60 pA in the soma (*left traces*), or 90 pA in a dendritic compartment at 390 μm (*right traces*). After a 200-ms interval without stimulation, a test AP was elicited with a short (90 pA, 70 ms) current pulse. (*C*) Steady-state activation for the gating variable of the shunting conductance, f, and its time constant, τ_f. (*D*) Steady state for the gating variables of the Na^+ conductance, l, n, and i (——), and their time constants τ_l, τ_n, and τ_i (·····). – – –, Steady-state inactivation, r, of the I_{Na}-dependent current $I_r = -I_{Na}r$.

Kinetic properties needed to model the activity-dependent changes of dendritic APs

The characteristics of the mechanism responsible for the activity-dependent changes in the APs in the dendrites can be inferred by looking at the experimental results (Spruston et al., 1995). Our aim is to implement a model in good qualitative agreement with those experiments, suggesting why the amplitude of APs in the apical dendrites of CA1 neurons changes during and after a somatic or dendritic current injection. Let us consider the voltage dependence of a hypothetical mechanism:

- The mechanism was substantially activated by a few APs. The recovery time was long at resting potential and was reduced with hyperpolarization. Thus the time constant for activation must be fast for depolarized membrane potentials; deactivation should be on the order of seconds around resting potentials and must accelerate with hyperpolarization.
- Once the mechanism was activated it remained active during the entire duration of the current injection (~1 s), even if the amplitude of the APs was already drastically reduced after the first few APs, and no signs of its deactivation were observed (such as an increase in the amplitude of the APs toward the end of the stimulation). A half-activation value of $V_{1/2} \approx -55$ mV would be consistent with this observation. In fact, the value of $V_{1/2}$ determines the effects of the mechanisms near the resting potential. A $V_{1/2}$ that is too high with respect to resting potential would result in a deactivation of the mechanism during long suprathresold stimulations, whereas a $V_{1/2}$ that is too low would result in a mechanism that is already active at rest (in contrast with the experiments showing that the first AP is not affected).
- Somatic injection of negative currents showed only a hyperpolarization followed by a slow relaxation. This is the typical I_h-dependent sag (Spruston and Johnston, 1992). Thus the current generated by the mechanism must shut off rapidly (or reduce to a very small level) with hyperpolar-

ization. It cannot be large and it should be constant over the entire hyperpolarization range, otherwise there should be some visible effect for different levels of negative current injection (such as distortion or disappearance of the sag).

- Its reversal potential, E_{rev}, should not be significantly different from the resting potential. In fact, E_{rev} much lower than the resting potential (such as for K^+ currents) would result in an increasing after-hyperpolarization (AHP) at the end of each spike, and in a big and long AHP at the end of the stimulation, in contrast with experiments. On the other hand, E_{rev} much higher than the resting potential would be in contrast with experimental findings on distal dendrites for long somatic stimulation. In fact, for the latter case, the mechanism should be open and working during the entire stimulation period, even if the "failed" APs are not higher than about 20 mV.

We used these properties with two different mechanisms to model the attenuation and failures of APs in the dendrites: 1) a shunting conductance and 2) a reduction in sodium current, due to a slow sodium current inactivation. They share essentially the same kinetic characteristics for the key gating variable and its time constant. The definition of a failure is essentially arbitrary, and we have chosen to define a failure as a ~50% or more reduction in the amplitude of any two consecutive APs. In this work we assumed that both the attenuation and the failure of an AP in the dendrites are caused by the same mechanism.

To keep the model as simple as possible, only Na^+ and K^+_{DR} conductances (g_{Na} and g_{KDR}) were used to shape an AP in our cell. We have chosen to limit the set of additional active conductances to those strictly needed to roughly account for the specific features of CA1 neurons seen in the experiments (Spruston et al., 1995), such as the *h*-dependent sag and a small firing accommodation. The *h*-dependent sag was modeled with a nonspecific ionic conductance, g_h, whereas the small firing accommodation was modeled with a K^+ conductance, g_{KM}, that is known to be responsible for the Ca^{2+}-independent accommodation shown by CA1 neurons (Madison and Nicoll, 1984). The details of their kinetics are reported in the Appendix. We tested several different sets of densities and distributions for the two mechanisms, obtaining the same qualitative results. However, we have chosen to simulate the simplest case using, unless otherwise noted, the more conservative and stringent option of uniform density, distribution, and kinetic characteristics of channels in the soma and in all active dendritic compartments, without any specific dependence on geometry or distance from the soma. There was no shunting conductance or slow sodium inactivation at the axon.

Channel kinetics and distribution

Shunting conductance

A nonspecific ionic current $I_f = \bar{g}_f f$ was modeled and inserted in the soma and in all active dendritic compartments, with a constant density $\bar{g}_f = 7.5$ mS/cm^2. One of the key features of the gating variable f of this current (Fig. 1 *C*) is the separation between the voltage for which there is half activation of f, and the voltage at which the time constant τ_f peaks. One of the experimental findings, namely that lower current injection produces less attenuation (Spruston et al., 1995), depends on this separation. This feature could usually be modeled by using a higher power for the gating variable in the expression for the current. However, this can account for only a minor separation (up to ~5 mV). Bigger differences cannot be taken into account with the usual HH scheme, and a more complicated multistate model must be used. Because it was not a goal of this work to find a microscopic description of this conductance, we did not follow any specific kinetic scheme to implement the voltage dependence characteristics of the f gating variable and its time constant, τ_f.

Sodium conductance (g_{Na})

The kinetics of fast activation and inactivation of single Na^+ channels have recently been investigated in CA1 dendrites (Magee and Johnston, 1995), and their characteristics did not appear to be very different from those at the soma. Our activation and inactivation gating variables (Fig. 1 *D*) are based on those results (see the Appendix). However, it has been shown experimentally in rabbit Schwann cells (Howe and Ritchie, 1992) and in hippocampal CA1 neurons (Kuo and Bean, 1994) that sodium inactivation may require a kinetic scheme more complex than that modeled with a single gating variable. We were primarily interested to show, in the simplest way, that a slow sodium inactivation could, in principle, account for the activity-dependent changes of dendritic APs. Hence we did not attempt to derive or implement an accurate multistate kinetic model of sodium inactivation, but simply added another gating variable, i, to the more conventional HH kinetic scheme used for Na^+ channels, an approach already followed by Fleidervish et al. (1996) to model slow cumulative spike adaptation in neocortical neurons. Essentially the same kinetic characteristics of f (the gating variable of the shunting conductance) were used for i, together with an adjustable parameter (b_i, see the Appendix) to limit the maximum allowed amount of slow inactivation ($b = 1$ no inactivation, $b = 0$ maximum inactivation). In agreement with experimental findings, a uniform density for $\bar{g}_{Na}$ was used in all active compartments ($\bar{g}_{Na} = 20$ mS/cm^2). It has been shown experimentally that, with a dendritic or a somatic stimulation, an AP is elicited at or near the axon first, and then it back-propagates in the soma and dendrites (Stuart and Sakmann, 1994; Spruston et al., 1995). This effect has recently been modeled using a very high density of Na^+ channels in the axon (Mainen et al., 1995). For the axon in our model we used a 50-fold increase in the Na^+ channel density and $R_a = 50$ Ωcm. In addition, in the experiments (Spruston et al., 1995) an AP was initiated at the soma for low dendritic current injection and in the dendrite for higher dendritic current injection. We found that a shift of the steady-state

activation and inactivation curves 5 mV to hyperpolarized potential in the axon was sufficient to be consistent with these experimental findings. Because it has been shown experimentally that phosphorylation could shift the activation and inactivation curves of many channels, including Na^+ (Ismailov and Benos, 1995), we did not consider this choice to be unrealistic. Experimental values for the kinetics parameters of Na^+ channel predict a small but significant Na^+ current near the resting potential. This results in a spontaneous depolarization of the cell from rest. In real (and stable) neurons, Na^+ current active near rest does not produce such depolarizations. To model this situation, we simply included an additional nonspecific I_{Na}-dependent current, $I_r = -I_{Na}r$. The voltage dependence of the state variable r is shown in Fig. 1 *D* (*right*), and its instantaneous value is assumed to be always in equilibrium with its steady-state value. The reason to include the sodium-dependent current was to maintain the parameters for the activation and inactivation curves of the Na^+ channel as close as possible to the experimental values. By shifting to the right the voltage dependence of the kinetic curves of our model for Na^+, the sodium-dependent current would have been unnecessary, but the resulting activation and inactivation curves would not have been in agreement with the experiments. The purpose of I_r was to smoothly switch off I_{Na} below ~ -60 mV, and this could be considered as representative of any processes that may serve to reduce the effects of I_{Na} near the resting potential. Using this model for the Na^+ conductance, we were able to obtain APs in the axon under a somatic or dendritic stimulation that were actively back-propagated in the dendrites, with amplitude and timing in good qualitative agreement with the experimental findings.

g_{KDR}

A previously published model (Migliore et al., 1995) devised for CA3 pyramidal neurons was adapted for this work. Besides the fast Na^+ inactivation, this was the only conductance responsible for the fast repolarization of an AP. Its distribution follows g_{Na}, and a uniform density, $\bar{g}_{KDR} = 6$ mS/cm^2, was used for all of the involved compartments.

g_{KM}

The parameters originally used for this K^+ conductance to model CA3 firing (Migliore et al., 1995) have been slightly changed, to roughly account for the firing accomodation shown by CA1 neurons. It has been included only in the axon, with $\bar{g}_{KM} = 0.5$ mS/cm^2.

g_h

We based our model for this nonspecific ionic conductance on the experimental data for CA1 by Halliwell and Adams (1982). Because it activates at hyperpolarized potentials, its major role is to shape the prominent sag that is experimentally observed in CA1 under a hyperpolarizing current injection (Spruston and Johnston, 1992). Its distribution follows g_{Na} and g_{KDR}, with $\bar{g}_h = 1$ mS/cm^2.

RESULTS

Control simulations of APs evoked by current injection in the soma (60 pA, 500 ms) or dendrite (390 μm, 90 pA, 500 ms) are shown in Fig. 1 *B*, where no slow inactivation or shunting conductance was used. Membrane potential is shown for the soma and at a distal dendrite 390 μm from the soma. After a 200-ms interval, a single AP was elicited with a short (70 ms) current pulse. As can be seen, no reduction in the amplitude of the APs in the train was observed at either location for a somatic or dendritic stimulation. The same protocol of stimulation was used in the simulations reported in Fig. 2 using the shunting conductance, and in Fig. 3 using the slow sodium inactivation. Membrane potential is shown for the soma (*bottom traces*), and for locations (*arrows* in Figs. 2 and 3) at 150, 310, and 390 μm from the soma. The time course of the relevant gating variables, f for the shunting conductance and i for the slow

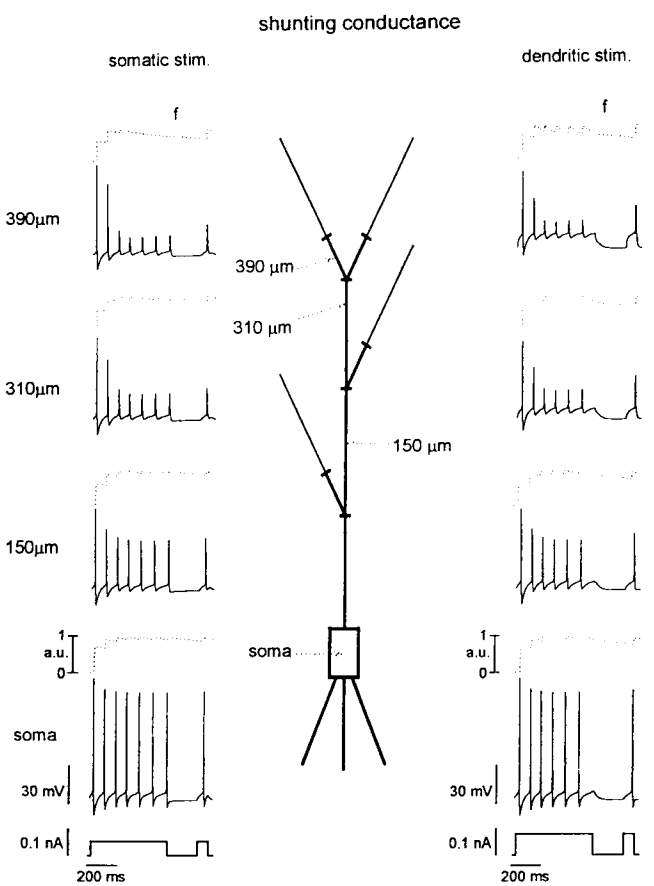

FIGURE 2 Simulation results, using a shunting conductance, for a somatic (*left traces*) or a dendritic (*right traces*) stimulation at the soma, at 150, 310, and 390 μm from the soma (locations indicated by the dotted arrows). The time course of the activation variable f is shown at each location (·····). Protocol of stimulation (*bottom*) as in Fig. 1 *B*.

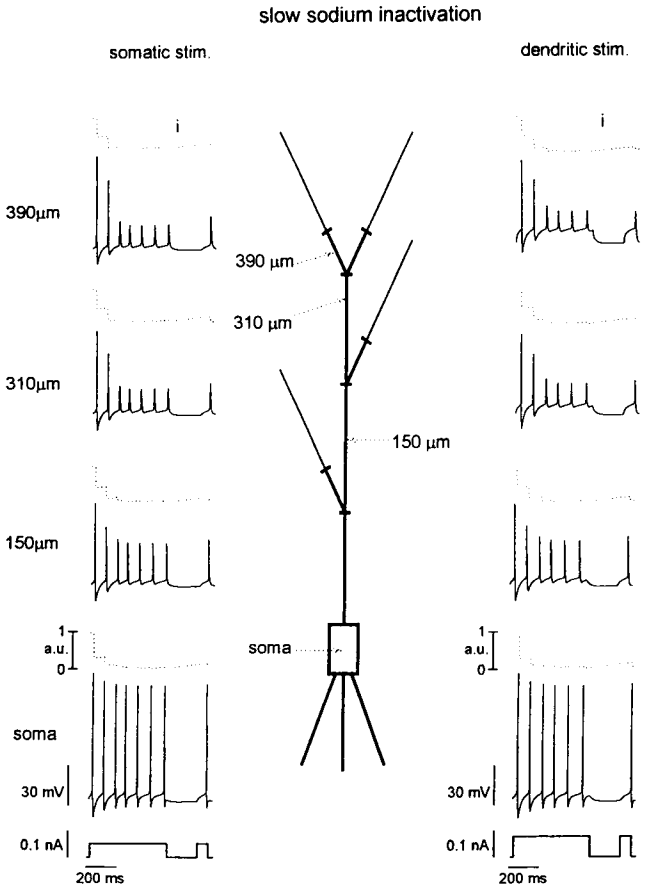

FIGURE 3 Simulation results, using the slow sodium inactivation, for a somatic (*left traces*) or a dendritic (*right traces*) stimulation at the soma, at 150, 310, and 390 μm from the soma (locations indicated by the *dotted arrows*). Protocol of stimulation (*bottom*) as in Fig. 1 *B*.

sodium inactivation, are also shown at each location (*dotted lines*).

With a shunting conductance (Fig. 2), only a negligible attenuation of the spike amplitude of successive spikes is observed at the soma, even if the gating variable, f, was almost completely activated after a few APs. An evident attenuation is already observed at 150 μm from the soma, and there is a failure to propagate more than 2 APs at 390 μm from the soma. Only partial recovery is observed after 200 ms without stimulation. The same qualitative results were observed for both somatic and dendritic stimulations.

Using the slow Na inactivation (Fig. 3), with the same protocol of stimulation, the results are qualitatively similar to those for the shunting conductance. However, the amplitude of the AP that "failed" to propagate in the dendrite at 390 μm is higher than those observed using the shunting conductance (~20 mV versus ~10 mV). In this case, the amplitude was essentially determined by the passive propagation of the APs from the parent compartment. In fact, the local Na^+ current is almost completely inactivated ($i \simeq 0$), preventing a significant local active contribution to the amplitude of an AP.

For both mechanisms, the amplitude of the first AP measured at 390 μm from the soma was different for a somatic or a dendritic stimulation (*top traces* in Figs. 2 and 3). In particular, the peak of the first AP was lower for a dendritic stimulation. The reason for this effect is in the ~10-mV depolarization caused by a dendritic stimulation, which precedes the invasion of a back-propagated AP in the dendrite. This depolarization had two consequences: 1) g_{Na} was forced in a more inactivated state (compare the values of the fast sodium inactivation gating variable l at −65 and −55 mV, Fig. 1 *C*), and 2) there is a larger (~ +20%) activation of the mechanism responsible for the attenuation.

The effects of hyperpolarization and of different levels of depolarization on the amplitude of APs at 390 μm are shown in Fig. 4 *A* (using the shunting conductance) and in Fig. 4 *B* (using the slow sodium inactivation). Membrane potential (*solid lines*) and the appropriate gating variable (*dotted lines*) are shown in simulations where a test AP was elicited after different conditioning stimulations (Fig. 4 *B*, *bottom*). In one case (*panels c* in Figs. 4, *A* and *B*) a superposition of several simulations is shown. In agreement with experiments (see figure 3 in Spruston et al., 1995), a subthreshold stimulation (31 pA, Fig. 4, *Aa* and *Ba*) did not result in any significant reduction of the test AP, whereas suprathreshold stimulations (66 pA, Fig. 4, *Ab* and *Bb*; 90 pA, Fig. 4, *Ac* and *Bc*) resulted in attenuation of the test AP that lasted longer when more APs were elicited during the initial 500-ms conditioning. The time course of the gating variables during hyperpolarization (−0.5 nA, Fig. 4, *Ad* and *Bd*) clearly shows that their faster deactivation during hyperpolarization allowed for the faster and almost complete recovery of the AP amplitude, in agreement with experiments.

The effects of the two mechanisms on an AP that failed to propagate into a dendritic branch at 390 μm from the soma are shown in Fig. 5. The last spikes at the end of the 500-ms somatic current injection in Figs. 2 and 3 are superimposed along with a simulation where we used $\bar{g}_{Na} = 0$ everywhere except in the axon, to model the passive propagation of an AP into the same compartment. As can be seen, the AP evoked in the model with the slow sodium inactivation had a larger amplitude, because this mechanism simply reduces the Na^+ current. In contrast, the shunting conductance resulted in the greatest attenuation of the AP.

Fig. 6 illustrates a possible experimental test of whether the Na^+ channel inactivation mechanism is involved in the activity dependence of AP back-propagation. The simulations show the sodium current through a 2-μm^2 membrane patch elicited by a repeated voltage clamping of the soma (*left traces*) and the compartment at 390 μm (*right traces*), using the shunting conductance and the slow sodium inactivation. As can be seen, only the latter showed a progressive reduction of the sodium current, and the effect is the same at the soma and at 390 μm.

It has been consistently found experimentally that failures are often localized after branch points, and in several cases, asymmetrical AP propagation after a branch point was indirectly revealed by imaging the intracellular calcium

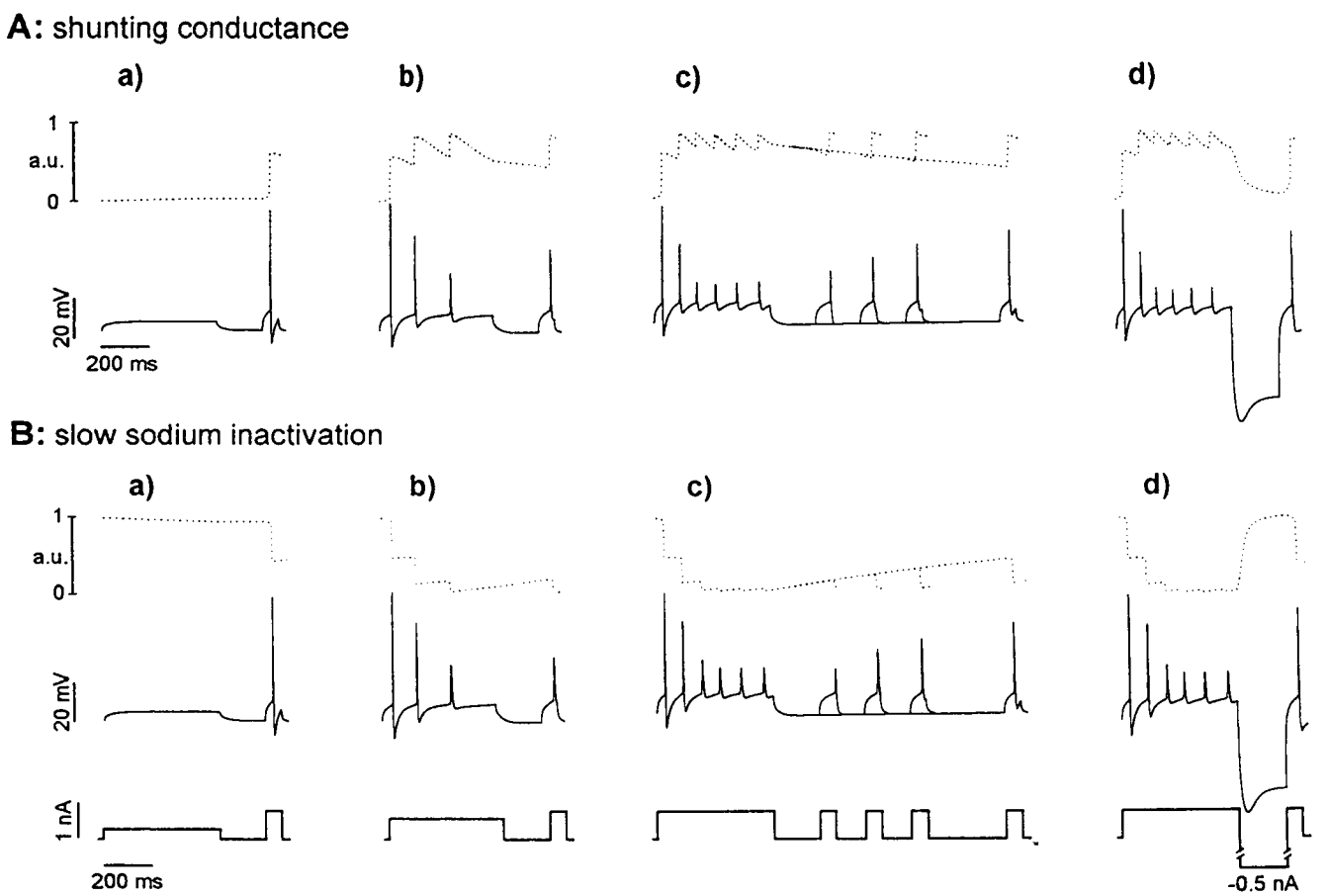

FIGURE 4 Membrane potential at 390 μ from the soma (——) and gating variables (·····, f for the shunting conductance and i for the slow sodium inactivation) during simulations using different protocols of dendritic stimulation (bottom). (*A*) results using the shunting conductance. (*B*) Results using the slow sodium inactivation. In all cases a test AP was elicited at the end of the conditioning period with a short (90 pA, 70 ms) current pulse. (a) Subthreshold current injection (31 pA, 500 ms) followed by 200 ms without stimulation; (b) suprathreshold current injection (65 pA, 500 ms) followed by 200 ms without stimulation; (c) superposition of four simulations using suprathreshold current injection (90 pA, 500 ms) followed by 200, 400, 600, or 1500 ms without stimulation; (d) Suprathreshold current injection (90 pA, 500 ms) followed by hyperpolarization (−0.5 nA, 200 ms).

concentration (see figure 5A in Spruston et al., 1995). This suggests that changes in the local properties of the membrane, at or after a branch point, could result in an asymmetrical failure of AP propagation. To determine the conditions under which our model predicts such experimental findings, we modified the passive parameters of the model in such a way as to obtain attenuation (rather than failure) at 390μm from the soma, and found what changes in the local properties of one branch resulted in a failure in the propagation of APs. The results of the simulations are shown in Fig. 7 and Fig. 8, using the shunting conductance and the slow sodium inactivation, respectively. As initial conditions, we started with a lower value for the maximum density of the shunting conductance ($\bar{g}_f$ = 6.5 mS/cm^2), and limited to 90% of its maximum the slow Na^+ inactivation (b_i = 0.1). A somatic current injection (70 pA, 400 ms) was used to evoke a train of APs that propagated up to the last compartment of the apical dendritic trunk (d0 in Figs. 7 and 8) and to its daughter compartments (d1 and d2). Under these conditions only attenuation was observed (Figs. 7*A* and 8*A*). The following changes were then applied to the d1 branch: a reduction in the diameter, from 1.9 to 0.1μm (Figs. 7 *B* and 8 *B*), an increase in R_a, from 200 to 3000 Ωcm (Figs. 7 *C* and 8 *C*), and a decrease in R_m from 8000 to 400 Ωcm^2 (Figs. 7 *D* and 8 *D*). Each of these modifications was a cause of strong impedance mismatch at the branch point and, as can be seen from Figs. 7 and 8, resulted in an asymmetrical failure of an AP.

DISCUSSION

We presented two models representative of two conceptually different classes of mechanisms that could independently account for the degradation in the information contained in a train of APs traveling from the soma to the dendritic tree. The simulations suggested that a specific property of Na^+ channels, slow inactivation, and/or a nonspecific ionic shunting conductance could, in fact, be responsible for the dynamic changes that have been experimentally shown to occur in hippocampal CA1 neurons.

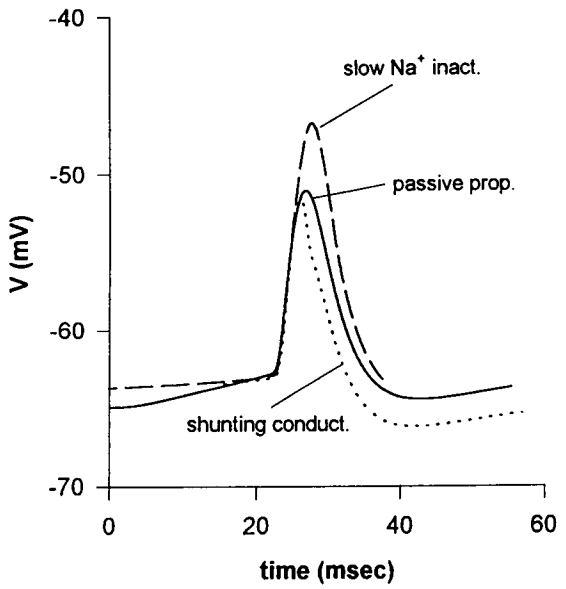

FIGURE 5 Superposition of the passive propagation of a somatic AP in a dendritic compartment 390 μm from the soma ($g_{Na} = 0$, ——), with the failure caused by the shunting conductance (·····) or by the slow sodium inactivation (– – –), during a somatic stimulation (the last peaks of the train in top left traces of Figs. 2 and 3 were used for the comparison).

A few considerations on the properties of the two mechanisms

It was not necessary to use any specific ionic channel in our model other than those strictly required to generate an AP and some other electrophysiological characteristics of CA1 cells, such as the sag (modeled with the g_h) and a weak accommodation (modeled with the g_{KM}). The model predicts, therefore, that the observed activity-dependent changes should be quite robust and rather insensitive to pharmacological block of many different ionic channels that, with this model, do not play any role. Furthermore, although voltage-gated potassium channels could dynamically change the dendritic cable properties and affect synaptic transmission (Wilson, 1995), we think they should be ruled out as shunting conductance in our case. In fact, we carried out several preliminary simulations of a shunting conductance using the typical reversal potential of K^+ channels (~ -90 mV) with several different sets of densities and distributions. However, the low reversal potential resulted in a strong accommodation during the stimulation, a big AHP at the end of each spike, and a big and long AHP at the end of the stimulation, in contrast with experiments. Another possible candidate as shunting conductance could be feedforward inhibition. In fact, there is some experimental evidence that favors this hypothesis. In CA3 it has been shown that disynaptic inhibition can occur with a latency as small as 3–5 ms, and it could suppress burst discharge (Traub et al., 1994). GABA-dependent Cl^- channels have been suggested as a cause of transmission failures in axonal arborization (Wall, 1995) and AP blockade in nerve terminals (Zhang and Jackson, 1993). Whether inhibition is a cause also for the activity-dependent changes in AP propagation could be experimentally tested by examining whether AP back-propagation failures are altered or relieved after bicuculline application.

One of the key characteristics of both mechanisms is that they have some "memory" of the past history of the cell (represented by the slow deactivation time constant). Because the level of intracellular calcium could be considered a measure of the past activity of a neuron, it may work as "memory," as suggested by Lüscher et al. (1994), for dorsal root ganglion cells. Thus it could be one of the mechanisms involved with attenuation and failure, but 1) there is little experimental evidence for the kind of voltage-dependent extrusion of Ca^{2+} suggested by the experiments on hyperpolarization, and 2) with distance from soma, $[Ca^{2+}]_i$ after a train decreases, whereas attenuation and failures increase.

The simulations of the Na^+ current from somatic or dendritic patches (Fig. 6) suggested a way to distinguish between a shunting conductance or a slow sodium inactivation as the cause of activity-dependent AP changes and showed that it should not be necessary to patch a distal dendrite for this purpose, assuming that the properties and density of sodium channels are the same at the soma and at the dendrites.

It is interesting to note that, with this model, the simple activation of the mechanisms that could produce attenuation and/or failures is not a sufficient condition to show these effects. As suggested from the simulations in Figs. 2 and 3, electrotonic distance from the site of AP initiation is also a necessary condition. In fact, because of the current flowing from the axon, there is no attenuation at the soma, even if both mechanisms are fully activated.

Another suggestion of the model is on the effects of pharmacological block of one or more K^+ channels. Membrane potential is already partially shunted by the plethora of K^+ channels normally present on a dendrite. Their pharmacological block usually results in an increase in the firing frequency (Madison and Nicoll, 1984). Because the activation of our mechanisms depends on the firing frequency (Fig. 4), an increase in the activity-dependent changes is predicted by our model in this case.

On the conditions for failures

With this model, a slow sodium inactivation cannot result in an AP lower than a passively propagated one, and the Na^+ inactivation simply tends to reduce the AP to the amplitude it would have in a passive neuron (Fig. 5). This suggests that the shape of an AP that failed to propagate in a dendritic compartment may give some information on which mechanism is responsible for failure. In fact, comparison of the "failed" APs with a passive propagation of somatic spike, such as that obtained by the use of tetrodotoxin on an extended portion of the apical dendritic tree, could show whether spikes are truncated.

In the experiments on CA1 neurons, branch points appeared to be the preferential location for failures. With the

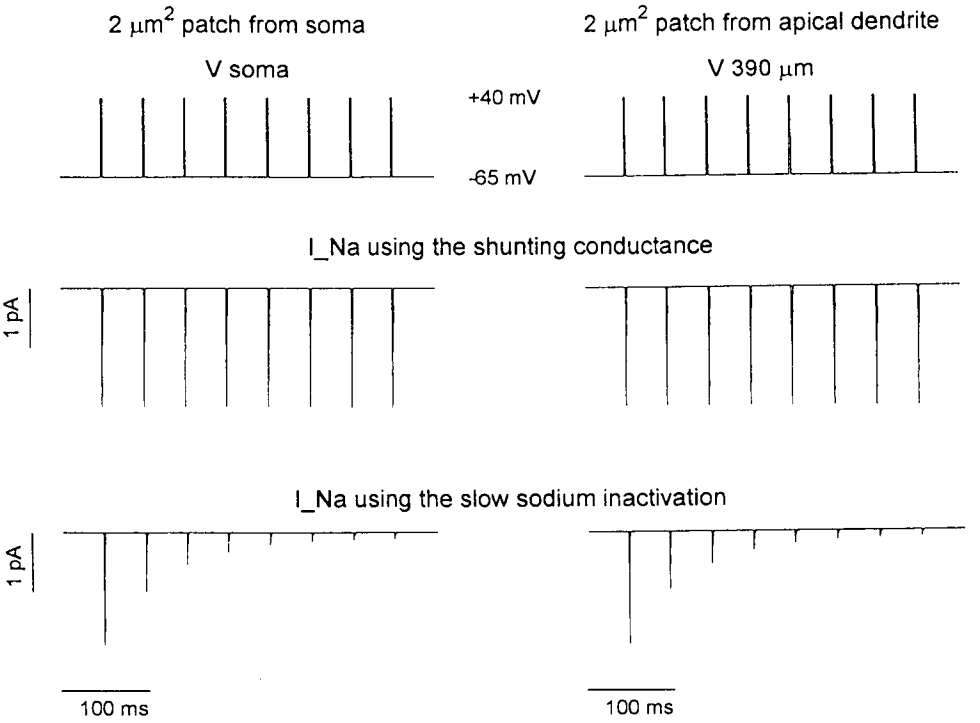

FIGURE 6 Effect of voltage clamp on the sodium current. The soma (*left traces*) or the compartment at 390 μm are held at −65 mV and clamped at +40 mV for 2 ms at 20 Hz (*top*). The sodium current elicited from this protocol, as measured from a 2-μm^2 membrane patch, is shown in two simulations using the shunting conductance (*middle*) and the slow sodium inactivation (*bottom*).

uniform densities and distributions we used in most simulations (Figs. 2–6), however, branch points do not have special features because they were not a necessary condition for failure of AP propagation. In fact, an unbranched parallel compartment, at the same distance from soma, showed essentially the same features of AP amplitude (simulations not shown) in Figs. 2 and 3. Asymmetrical failures at branch points could, however, be facilitated by a drastic impedance mismatch at particular branch points (Figs. 7 and 8), where changes in the morphological or in the passive properties in one branch led to localized failures. It should be noted that, besides being an index of the robustness of the model for changes in the morphological and passive model parameters, we have considered these changes for illustrative purposes. In fact, it was important to show that the model was able to reproduce asymmetrical failure in the most stringent case, such as when only a single parameter is changed, and that this was true for all three parameters. In some additional simulations we verified that a fourfold change in all three parameters resulted in an asymmetrical failure. If one also considers that in real neurons two daugther branches could have different densities of Na^+ channel and/or shunting conductance, and/or additional hyperpolarizing conductances, it is easy to understand that the relative changes need not be very big. It is possible to test experimentally to determine which one of these factors is in effect in real neurons, by selective synaptic activation of two daughter dendrites after a branch point to compare for differences in the excitatory post-synaptic potential at the soma, by a direct measure of the local input resistance after a branch point, or by using 3D reconstruction of a neuron with known electrophysiology to find correlations between locations of failures and branch diameter (a deep analysis of the effects of step changes in the diameter of a core conductor on an AP was carried out by Goldstein and Rall, 1974).

CONCLUDING REMARKS

Finally, it should be noted that the model was in very good agreement with experimental data, despite the fact that we used the two mechanisms in a very simple model cell that consisted of a reduced geometry, a limited set of active conductance, and a uniform density and distribution of channels in the soma and dendrites. Additional factors, such as more complicated dendritic branching geometry, additional conductances, and nonuniform channel distribution and density, may result in a richer variety of conditions with potentially important consequences for how a dendritic tree selectively process the massive amount of information propagating throughout a neuron.

APPENDIX: CHANNEL KINETICS

Unless otherwise noted, $x_\infty = \alpha_x/(\alpha_x + \beta_x)$ and $\tau_x = 1/(\alpha_x + \beta_x)$, where x is a gating variable, v is in mV, and $W = 10^{-3}F/RT$.

$$I_f = \bar{g}_f \cdot f \cdot (v + 55), \qquad I_f = 0 \quad \text{for} \quad v < -55$$

$$f_\infty = 1/(1 + \exp(-(v - 55)/2))$$

$$\alpha_f = 4 \cdot 10^{-4}\exp(9.6(v + 65)W)$$

$$\beta_f = 4 \cdot 10^{-4}\exp(-2.4(v + 65)W)$$

$$\text{If} \quad \tau_f < 3 \quad \text{then} \quad \tau_f = 3 \text{ ms}.$$

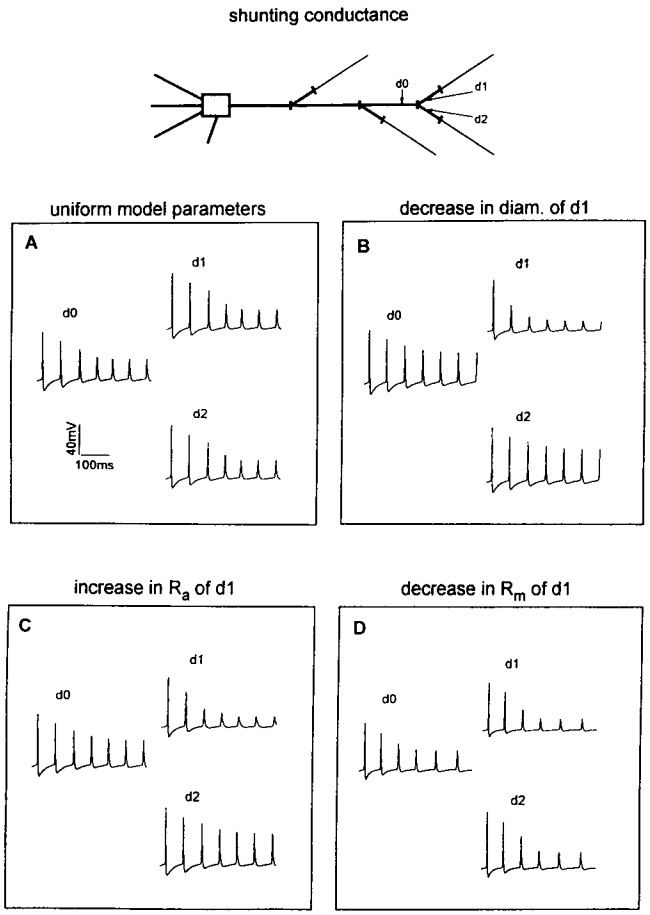

FIGURE 7 Simulations of asymmetrical action potential failures after a branch point, with a shunting conductance. The membrane potential is shown, at 310 μm (d0) and in two daughter branches (d1 and d2) at 390 μm. A uniform density for $\bar{g}_f$ = 6.5 mS/cm^2, and the same somatic stimulation (70 pA, 400 ms) was used in all cases, with (*A*) uniform model parameters, (*B*) diameter of d1 reduced from 1.9 to 0.1 μm, (*C*) R_a in d1 increased from 200 to 3000 Ωcm, and (*D*) R_m in d1 decreased from 8000 to 400 Ωcm^2.

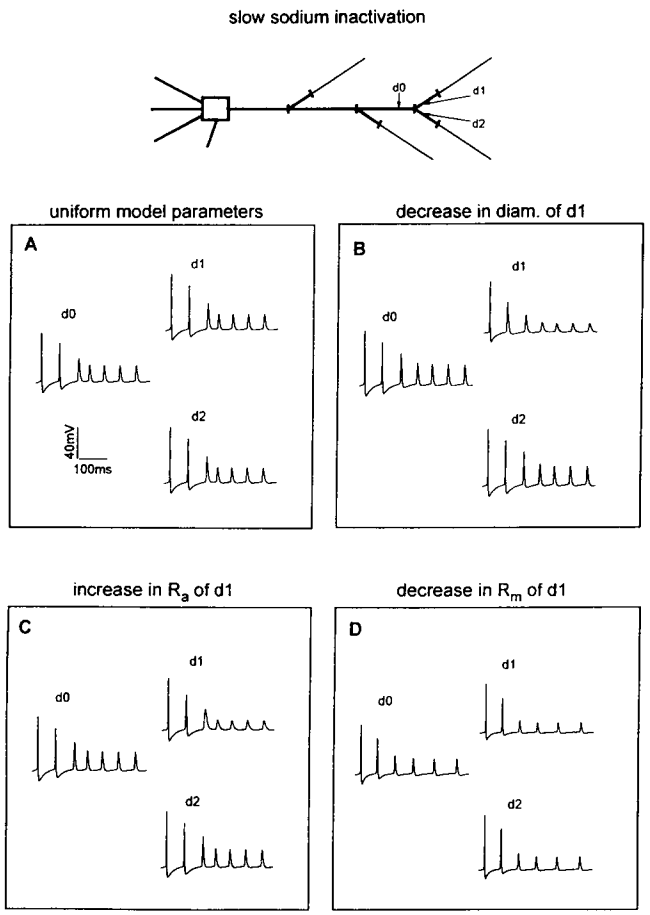

FIGURE 8 Simulations of asymmetrical action potential failures after a branch point with the slow sodium inactivation, using b_i = 0.1 in *A* to model attenuation as initial condition. The same protocol of stimulation and changes in the local model parameters as in Fig. 7 were used.

$$I_{Na} = \bar{g}_{Na} \cdot n \cdot l \cdot i \cdot (v - 50)$$

$$\alpha_n = 2.76 \exp(0.9 \cdot 4 \cdot (v + 30)W)$$

$$\beta_n = 2.76 \exp(-0.1 \cdot 4 \cdot (v + 30)W)$$

$$\alpha_l = 0.14 \exp(-0.65 \cdot 4 \cdot (v + 57)W)$$

$$\beta_l = 0.14 \exp(0.35 \cdot 4 \cdot (v + 57)W)$$

$$i_\infty = (1 + b_i \exp((v - 58)/2))/(1 + \exp((v - 58)/2))$$

$$\alpha_i = 4 \cdot 10^{-4} \exp(9.6(v + 60)W)$$

$$\beta_i = 4 \cdot 10^{-4} \exp(-2.4(v + 60)W)$$

$$I_r = -I_{Na} \cdot r$$

$$r_\infty = 1/(1 + \exp(-20(v + 50)W))$$

$$\text{If} \quad \tau_n < 0.02 \quad \text{then} \quad \tau_n = 0.02 \text{ ms.}$$

$$\text{If} \quad \tau_l < 1 \quad \text{then} \quad \tau_l = 1 \text{ ms.}$$

$$\text{If} \quad \tau_i < 3 \quad \text{then} \quad \tau_i = 3 \text{ ms.}$$

$$I_{K_M} = \bar{g}_{K_M} \cdot m \cdot (V + 91)$$

$$\alpha_n = 7.2 \cdot 10^{-4} \cdot \exp(0.8 \cdot 7 \cdot (V + 55) \cdot W)$$

$$\beta_m = 7.2 \cdot 10^{-4} \cdot \exp(-0.2 \cdot 7 \cdot (V + 55) \cdot W)$$

$$\text{If} \quad \tau_m < 10 \quad \text{then} \quad \tau_m = 10 \text{ ms.}$$

$$I_h = \bar{g}_h \cdot q \cdot (v + 55)$$

$$\alpha_q = 2.8 \cdot 10^{-3} \exp(-0.4 \cdot 5 \cdot (v + 93)W)$$

$$\beta_q = 2.8 \cdot 10^{-3} \exp(0.4 \cdot 5 \cdot (v + 93)W)$$

$$I_{K_{DR}} = \bar{g}_{K_{DR}} \cdot n^3 \cdot l \cdot (v + 91)$$

$$\alpha_n = 0.06 \exp(0.7 \cdot 5 \cdot (v + 40)W)$$

$$\beta_n = 0.06 \exp(-0.3 \cdot 5 \cdot (v + 40)W)$$

$$\alpha_l = 0.002 \exp(-1 \cdot 2 \cdot (v + 60)W)$$

$$\beta_l = 0.02$$

$$\text{If} \quad \tau_n < 0.3 \quad \text{then} \quad \tau_n = 0.3 \text{ ms.}$$

I thank D. Johnston and N. Spruston for many important suggestions and helpful discussions.

This work was supported by the Consiglio Nazionale delle Ricerche (CNR) "Programma di Scambi Internazionali."

REFERENCES

Andreasen, M., and J. D. C. Lambert. 1995. Regenerative properties of pyramidal cell dendrites in area CA1 of the rat hippocampus. *J. Physiol. (Lond.).* 483.2:421–441.

Borg-Graham, L. J. 1991. Modelling the non-linear conductances of excitable membranes. *In* Cellular Neurobiology: A Practical Approach. J. Chad and H. Wheal, editors. New York: IRL Press. 247–275.

Callaway, J. C., and W. N. Ross. 1995. Frequency dependent propagation of sodium action potentials in dendrites of hippocampal CA1 pyramidal neurons. *J. Neurophysiol.* 74:1395–1403.

Fleidervish, I. A., A. Friedman, and M. J. Gutnick. 1996. Slow inactivation of Na^+ current and slow cumulative spike adaptation in mouse and guinea pig neocortical neurones in slices *J. Physiol. (Lond.).* 493.1: 83–97.

Goldstein, S. S., and W. Rall. 1974. Changes of action potential shape and velocity for changing core conductor geometry. *Biophys. J.* 14:731–757.

Halliwell, J. V., and P. R. Adams. 1982. Voltage-clamp analysis of muscarinic exitation in hippocampal neurons. *Brain Res.* 250:71–92.

Hines, M. 1993. NEURON—a program for simulation of nerve equations. *In* Neural Systems: Analysis and Modeling. F. Eeckman, editor. Kluwer Academic Publishers, Norwell, MA. 127–136.

Howe, J. R., and J. M. Ritchie. 1992. Multiple kinetic components of sodium channel inactivation in rabbit Schwann cells. *J. Physiol. (Lond.).* 455:529–566.

Ismailov, I. I., and D. J. Benos. 1995. Effects of phosphorylation on ion channel function. *Kidney Int.* 48:1167–1179.

Kuo, C-C., and B. P. Bean. 1994. Na^+ channels must deactivate to recover from inactivation. *Neuron.* 12:819–829.

Lüscher, C., J. Streit, P. Lipp, and H-R. Lüscher. 1994. Action potential propagation through embtyonic dorsal root ganglion cells in culture. II. Decrease of conduction reliability during repetitive stimulation. *J. Neurophysiol.* 72:634–643.

Madison, D. V., and R. A. Nicoll. 1984. Control of the repetitive discharge of rat CA1 pyramidal neurones in vitro. *J. Physiol. (Lond.).* 354: 319–331.

Magee, J. C., and D. Johnston. 1995. Characterization of single voltage-gated Na^+ and Ca^{2+} channels in apical dendrites of rat CA1 pyramidal neurons. *J. Physiol. (Lond.).* 487:67–90.

Mainen, Z. F., J. Joerges, J. R. Huguenard, and T. J. Sejnowski. 1995. A model of spike initiation in neocortical pyramidal neurons. *Neuron.* 15:1427–1439.

Migliore, M., E. P. Cook, D. B. Jaffe, D. A. Turner, and D. Johnston. 1995. Computer simulations of morphologically reconstructed CA3 hippocampal neurons. *J. Neurophysiol.* 73:1157–1168.

Rudy, B. 1981. Inactivation in *Myxicola* giant axons responsible for slow and accumulative adaptation phenomena. *J. Physiol. (Lond.).* 312: 531–549.

Spruston, N., and D. Johnston. 1992. Perforated patch-clamp analysis of the passive membrane properties of three classes of hippocampal neurons. *J. Neurophysiol.* 67:508–529.

Spruston, N., Y. Schiller, G. Stuart, and B. Sakmann. 1995. Activity-dependent action potential invasion and calcium influx into hippocampal CA1 dendrites. *Science.* 268:297–300.

Stuart, G. J., and B. Sakmann. 1994. Active propagation of somatic action potentials into neocortical pyramidal cell dendrites. *Nature.* 367:69–71.

Traub, R. D., J. R. G. Jefferys, R. Miles, M. A. Whittington, and K. Toth. 1994. A branching dendritic model of a rodent CA3 pyramidal neurone. *J. Physiol. (Lond.).* 481:79–95.

Traub, R. D., and R. Llinás. 1979. Hippocampal pyramidal cells: significance of dendritic ionic conductances for veuronal function and epileptogenesis. *J. Neurophysiol.* 42:476–496.

Wall, P. D. 1995. Do nerve impulses penetrate terminal arborization? A pre-synaptic control mechanism. *Trends Neurosci.* 18:99–103.

Warman, E. N., D. M. Durand, and G. L. F. Yuen. 1994. Reconstruction of hippocampal CA1 pyramidal cell electrophysiology by computer simulation. *J. Neurophysiol.* 71:2033–2045.

Wilson, C. J. 1995. Dynamic modification of the dendritic cable properties and synaptic transmission by voltage-gated potassium channels. *J. Comput. Neurosci.* 2:91–115.

Zhang, S. J., and M. B. Jackson. 1993. GABA-activated chloride channels in secretory nerve endings. *Science.* 259:531–534.